18TH WORLD CONFERENCE ON EARTHQUAKE ENGINEERING
WCEE2024
MILAN

MILAN, ITALY
30TH JUNE - 5TH JULY 2024

www.wcee2024.it

POSSIBILITY OF THE EARTHQUAKE EARLY WARNING FOR THE 2023 TURKEY-SYRIA EARTHQUAKE

M. Yamada[1], Y. Xiao[2,3] & M. Morinaga[4]

[1] Disaster Prevention Research Institute, Kyoto University, Uji, Japan, masumi@eqh.dpri.kyoto-u.ac.jp

[2] Key Laboratory of Earthquake Engineering and Engineering Vibration, Institute of Engineering Mechanics, China Earthquake Administration, Harbin, China

[3] Key Laboratory of Earthquake Disaster Mitigation, Ministry of Emergency Management, Harbin, China

[4] Graduate School of Science, Kyoto University, Kyoto, Japan

Abstract: *On 6 February 2023 at 01:17(UTC), a large earthquake (Mw 7.8) struck southern and central Turkey, as well as northern and western Syria. The strong motions of these earthquakes were recorded by the Disaster and Emergency Management Authority (AFAD) in Turkey. We applied the earthquake early warning methods to the strong motion data, located the hypocenter, and estimated the rupture dimension. We applied three earthquake early warning algorithms: 1) the Extended Integrated Particle Filter (IPF) method to locate the hypocenter and estimate the magnitude, 2) the Propagation of Local Undamped Motion (PLUM) method to estimate the wavefield, and 3) XYtracker to estimate the fault rupture extent. The hypocenter was estimated at 4 s after the origin time with the location error less than 10 km. Based on the JMA standard, the EEW may be able to be provided to the public at 7 s after the origin time. The PLUM and XYtracker methods were able to capture the fault rupture extent which reduces the seismic intensity estimation errors. Assuming the strong motion data are available in real-time, these EEW methods can provide a warning to the public before the arrival of the severe shaking. It may contribute to mitigating the damage of large earthquakes.*

1 Introduction

On 6 February 2023, two large earthquakes struck southern and central Turkey, as well as northern and western Syria. The largest earthquake (Mw 7.8, hereafter referred to as mainshock) occurred at 01:17:34 (UTC), with maximum Mercalli intensity XII. The rupture extended bilaterally about 350 km along the main East Anatolian Fault Zone (Liu et al., 2023). The second largest earthquake (hereafter referred to as the largest aftershock), with Mw 7.5, occurred at 10:24:48 (UTC), following the mainshock 9 hours later. It ruptured the Sürgü Fault, part of the northern strand of the East Anatolian Fault Zone (Liu et al., 2023).

The strong motions of the earthquakes were recorded by the seismometers densely distributed along the fault. It is one of the most well-recorded large earthquakes (Mw>7.5) in the world. Large earthquakes are important for earthquake early warning systems because of the finite rupture and significant damage in wide areas. Such a large inland earthquake is less frequent so it is a valuable dataset.

In this study, we applied three earthquake early warning (EEW) algorithms to the dataset: 1) the Extended Integrated Particle Filter (IPF) method to locate the hypocenter and estimate the magnitude, 2) the Propagation of Local Undamped Motion (PLUM) method to estimate the wavefield, and 3) XYtracker to

estimate the fault rupture extent. Japanese earthquake early warning system currently uses the IPF and PLUM methods. We applied these methods to estimate the shaking intensities and discuss the possibility of the earthquake early warning system in Turkey.

2 Data

We used strong motion data recorded by the Turkey Disaster and Emergency Management Authority (AFAD). We obtained the data from the Turkish Earthquake Data Center System (TEDCS). There were about 300 seismic stations with 3 component accelerometers. We removed the data with incorrect clock (more than 10 s lag from the theoretical P-wave arrivals) and the data missing S-wave due to the communication loss. In total, we used 277 records for the mainshock. The Japanese EEW system uses the Japan Meteorological Agency (JMA) seismic intensity (SI) to estimate the ground motion at a site. The distribution of the SI of the mainshock is shown in Figure 1. The mainshock waveform alignment as a function of the epicenter distance is shown in Figure 2.

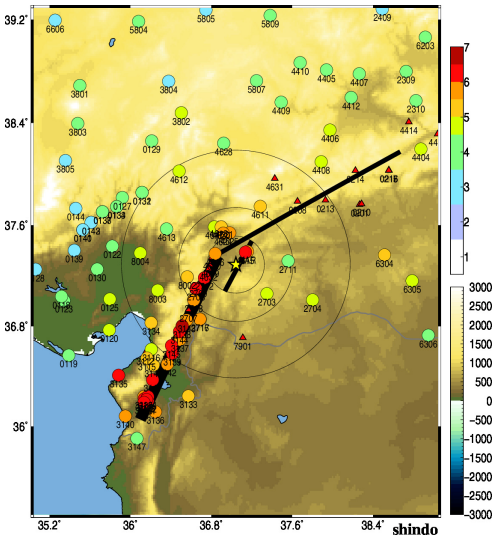

Figure 1. Observed SI. The thick lines show the fault line and the large circles show the R=25, 50, and 100 km from the epicentre. The background color indicates the altitude in m.

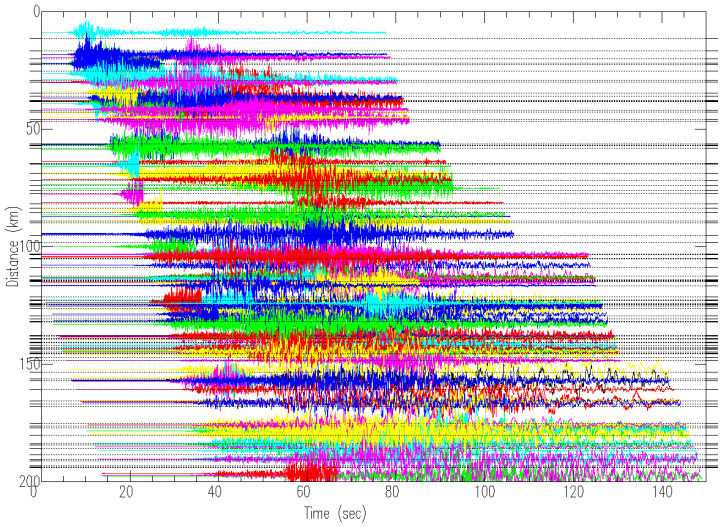

Figure 2. Acceleration waveforms in vertical component. They are aligned as a function of epicenter distance.

3 Method

3.1 IPFx method: point source determination algorithm

The IPFx method is a novel source determination algorithm developed for the EEW system (Yamada et al. 2021). It incorporates the smart phase association scheme and works well for sequential earthquakes (Yamada and Chen, 2022). During a period of active seismicity, such as that immediately following a large earthquake, phases from multiple earthquakes co-occur. This phase information has to be separated to accurately locate an earthquake. The phase association is performed based on the expected amplitude and arrival time. A similar method (IPF method) is currently used in the Japanese EEW system (Liu and Yamada, 2014; Tamaribuchi et al. 2014).

The algorithm comprises two steps: single-station processing and network processing. The single-station processing step extracts station trigger and amplitude information from continuous waveforms (Yamada and Mori, 2021), following which the network processing steps perform the source estimation from the extracted trigger and amplitude information based on Bayesian inference (Yamada et al. 2021). Both steps are performed in the central server so that we can adjust any type of data format and change the parameters easily. The IPFx method provides the hypocenter location and JMA magnitude. The ground motions at a site are estimated by the ground motion prediction equation used in the current Japanese earthquake early warning system (Japan Meteorological Agency, 2020).

3.2 PLUM method: wave-field estimation algorithm

The PLUM (Propagation of Local Undamped Motion) earthquake early warning (EEW) algorithm differs from typical source-based EEW algorithms as it predicts shaking directly from observed shaking without first deriving earthquake source information (e.g., magnitude and epicenter). The JMA seismic intensities are used to estimate the ground motion (Japan Meteorological Agency, 1996; Hoshiba et al., 2010). It is computed from the peak amplitude of the vector sum of the acceleration records band-pass filtered at ~0.5 Hz (Kunugi et al. (2013)).

Ground motion at a target site is estimated from the observations of the nearby stations (Kodera et al. (2018)).

$$I_{est}^{(k)} = \max_{i \in C_R}\{I_{obs}^{(i)} - a_0^{(i)}\} + a_0^{(k)} \quad (1)$$

Here, indexes i and k represent the spatial positions, $I_{est}^{(k)}$is the estimated SI at the estimation point k, and $I_{obs}^{(i)}$is the observed real-time SI at the station i. $a_0^{(i)}$ and $a_0^{(k)}$ denote the site amplification factors at i and k, converted into SI differences. For our analysis, the site amplification factors are unknown, so we did not consider them ($a_0^{(k)} = 0$). C_R is the circular region centered at the estimation point with radius R. The estimated SI at a target site is taken to be the maximum of the observed real−time SIs in a circular region of radius R.

In the Japanese earthquake early warning system, the radius R is set to 30 km, which is approximately equal to the average spatial interval of the seismic network. We tried to apply the same condition to the AFAD dataset, and it turned out that the number of stations within the radius is mostly less than 2. Therefore, we increased the radius R to 50 km. Figure 3 shows the number of stations within the radius at each target site. The coverage was greatly improved by increasing the radius.

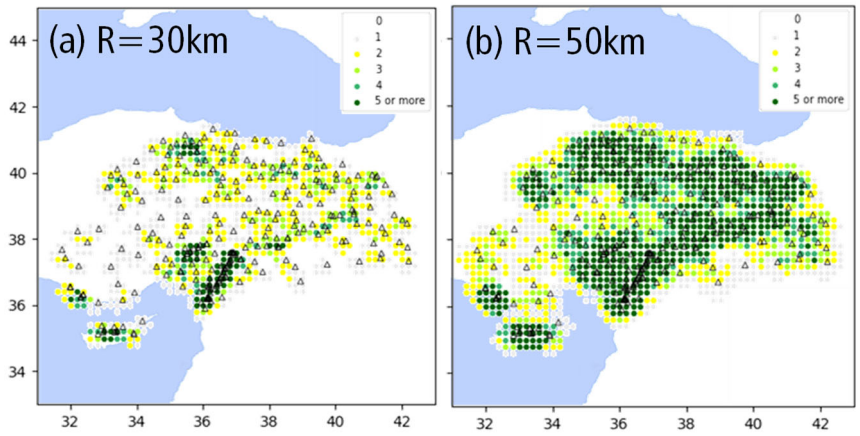

Figure 3. Number of the stations within the radius (a) 30km and (b) 50 km at each target site.

3.3 XYtracker: finite source determination algorithm

The XYtracker is a method to estimate fault rupture extent by a simple seismic intensity inversion (Xiao and Yamada, 2022). We assume three fault models: point-source (PS), line-source (LS), and rectangle-source (RS) model (Figure 4). The method is similar to the FinDer method (Böse et al., 2012) but it considers the fault width and evaluates the goodness-of-fit among three models.

Most of the EEW systems can detect the epicenter location soon after the earthquake occurs, so we assumed the epicenter was identified from the first few P-wave arrivals. The LS model was parameterized by three parameters, the length of the fault (L), the strike of the fault (θ), and the ratio of the length from the epicenter to one end along the strike (r_L). The RS model had an additional parameter, the width of the fault (W). We assumed that the epicenter was always at the center of the fault width to reduce the parameters.

We searched the most probable model parameters by minimizing the misfit function, defined by the residual sum of squares (RSS) between the observed and estimated seismic intensities:

$$\mathrm{RSS} = 1/n \sum_{i=1}^{n} \left[I_{obs}^{(i)} - I_{est}^{(i)} \right]^2 \quad (2)$$

where n is the number of stations where the observed seismic intensity is larger than 2.5, $I_{obs}^{(i)}$ and $I_{est}^{(i)}$ are observed and estimated JMA seismic intensities at the station i. $I_{est}^{(i)}$ can be estimated from the magnitude and fault distance, which is a function of model parameters (the detail is in Xiao and Yamada, 2022). We searched the most probable model parameters for LS and RS models that minimize the misfit function in equation (2).

We employed the AIC to select the most relevant source model among the PS, LS, and RS models (Akaike 1974). The AIC estimated the balance between the complexity of the models and the goodness of fit to the data:

$$\mathrm{AIC} = 2k + n \ln(\mathrm{RSS}) \quad (3)$$

where k represents the number of the free parameters and n also denotes the number of stations where the observed SI is 2.5 or greater. We use $k = 0$, 3, and 4 for the PS, LS, and RS models. The SI at a site is estimated by the same method as the current Japanese earthquake early warning system with a fault distance computed from the fault model.

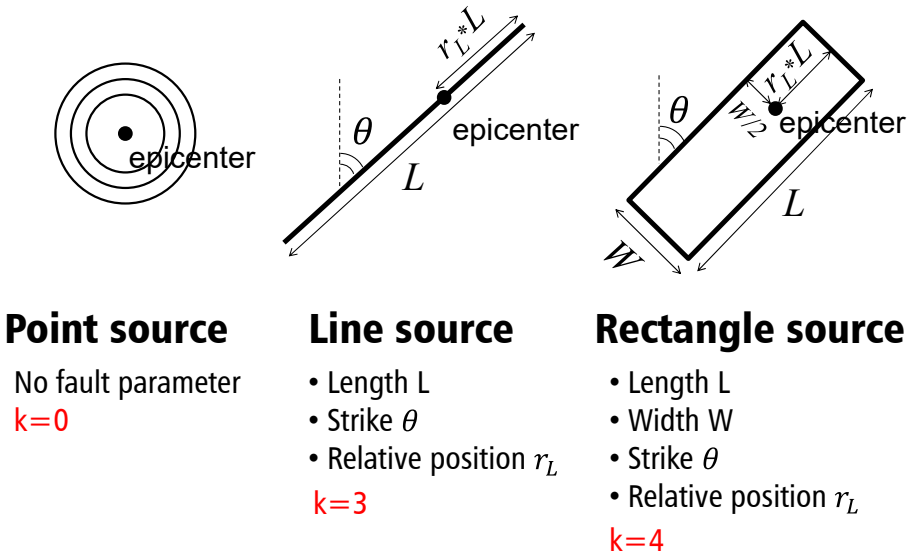

Figure 4. Diagrams of the geometry of the PS, LS, and RS models. The black circle shows the epicenter location

4 Results

4.1 IPFx method

Figure 5 shows the snapshot of the hypocenter estimation of the mainshock by the IPFx method. The IPFx method starts the estimation process when three stations are triggered. For the mainshock, three stations were triggered almost at the same time, and the hypocenter location was estimated (1:17:38). The estimated hypocenter location had a very small error (less than 10 km) at the first second. As more stations are triggered, the estimated location approaches the final catalog. Figure 6 shows the time history of the estimated source parameters. The hypocenter location is stable from the beginning of the processing when only a few stations are triggered. The estimated SI exceeds the threshold of public warning in Japan (4.5) 3 seconds after the first estimate (1:17:41). However, this IPFx method is based on the point source approximation, so it does not consider the finiteness. Figure 7 shows the estimated SI at the final time. Since we do not consider site amplification, the estimated SI decays in concentric circles. The SI was underestimated especially in the southwest direction where the fault rupture propagated.

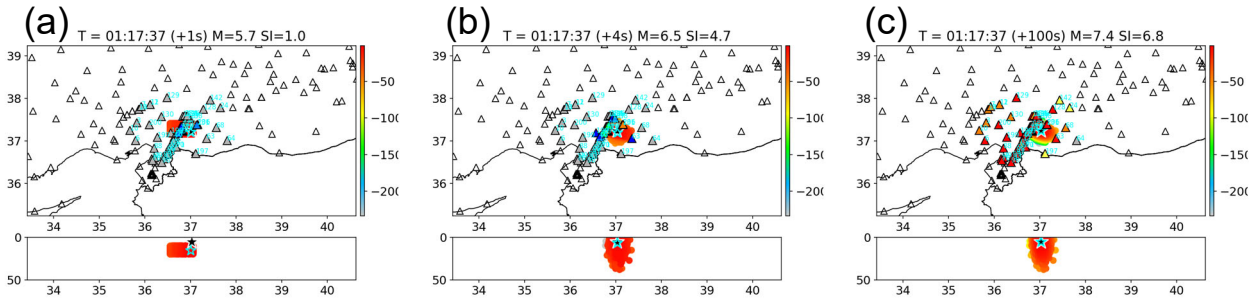

Figure 5. Hypocenter estimation by the IPFx method. T=1s, 3s, and 100s after the 3 stations were triggered (3s after the origin time) from the left. The triangles show seismic stations and colored triangles are triggered stations. The light blue and white star shows the estimated location at each time and the final, respectively. The color of the particles is proportional to the likelihood of the hypocenter location.

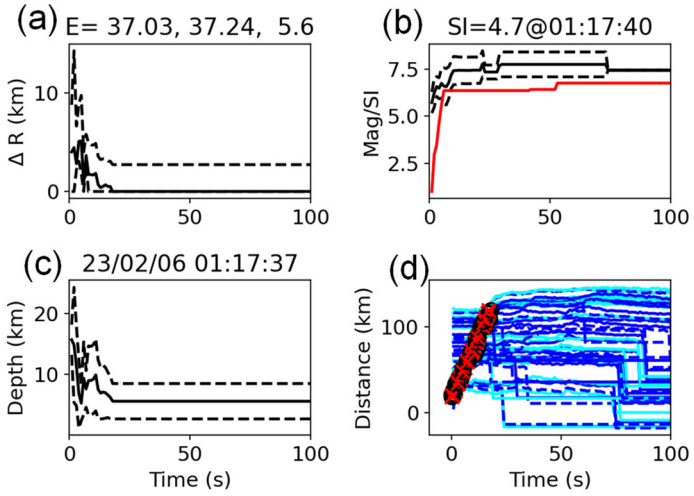

Figure 6. Time history of the estimates for source parameters by the IPFx method. The horizontal axis shows the time of processing. (a) Error of epicenter against the final estimation, (b) JMA magnitude (black) and maximum estimated shaking intensity (red), (c) epicenter depth, and (d) automatic picking time (black) and theoretical P-wave arrival time (red). Blue lines are SI amplitudes.

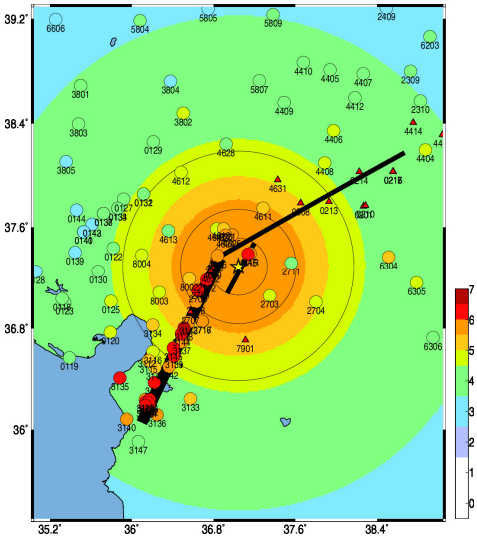

Figure 7. Estimated by the IPFx method.

4.2 PLUM method

Figure 8 shows the snapshot of the SIs observed and estimated by the PLUM method. The area with a large estimated SI gradually increases as the fault rupture propagates. At T=60s, the SI estimation properly captures the rupture direction in the southwest. Figure 9 shows the histogram of the warning time at each station. Assuming the threshold is SI=4.5, the warning time is defined as the difference between the observed and estimated SI when they exceed the threshold. The median of the warning time is 10.5s. Although the warning time is not so long, the accuracy of the estimation is high. Figure 10 shows the scatter plot of the observed and estimated SIs. The root mean square error is 0.83. It tends to be slightly overestimated since the PLUM method assumes no attenuation from the surrounding stations within R=50 km.

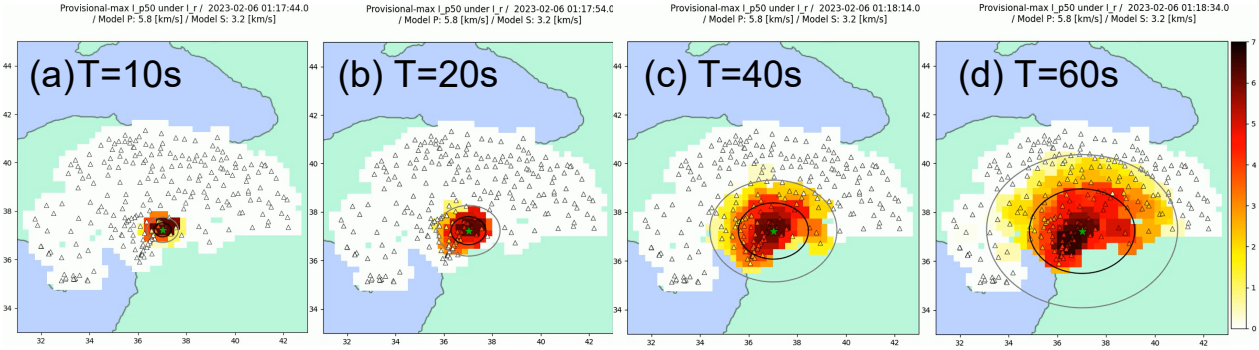

Figure 8. Snapshot of the SI estimates by the PLUM method. T=10s, 20s, 40s, and 60s after the origin time from the left. The triangles show the observed SI at that time and the background is the estimated SI. The large circles show P- and S-wave fronts.

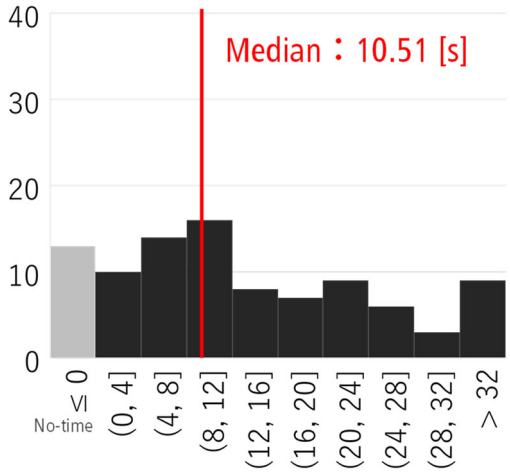

Figure 9. Histogram of the warning time at each station.

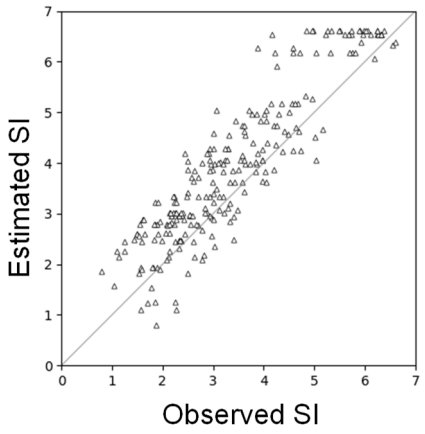

Figure 10. Observed and predicted SIs by the PLUM method.

4.3 XYtracker

Figure 11 shows the spatial distribution of the SIs observed and estimated by the XYtracker method. The high intensities were observed along the main East Anatolian Fault Zone in the southwest direction. LS and RS models could reproduce this directivity of the strong shaking. PS model significantly underestimated the SI in the southwest direction. Assuming the SI error within ±1 scale is acceptable, the accuracy for the PS model was 70%, and that for the LS and RS models were 88% and 83%, respectively. Figure 12 shows the time history of the source parameters and AIC. Based on the AIC model selection, the LS model was at 70 s after the origin time.

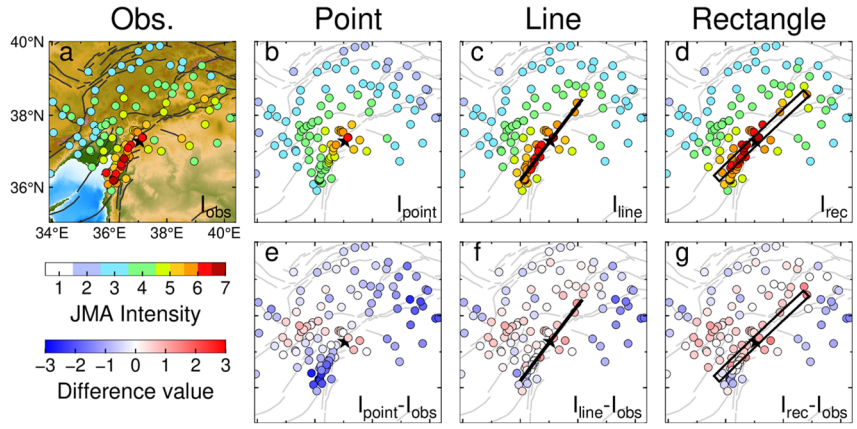

Figure 11. Distribution of the SI and its error at 150 s. The observation and the estimations of the PS, LS, and RS models are shown from the left. Black stars and thick lines show the epicenters and the source models, respectively. (a) Observed SI. (b)–(d) Estimated SIs for the 3 source models. (e)–(g) Difference between the estimated and observed SIs for the 3 source models. The red color indicates overestimated. and the blue color shows underestimated.

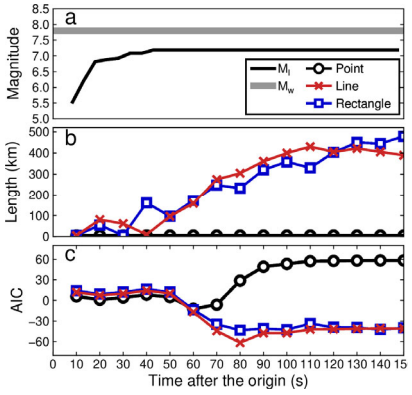

Figure 12 Time history of the source parameters and AIC. (a) Magnitude. (b) Length of the fault. (c)AIC.

5 Discussions

Figure 13 shows the snapshots of the SIs observed and estimated by the IPFx, PLUM, and XYtracker methods. The IPFx method is based on the point source model, so the estimated SI decays in concentric circles. The speed of the warning is the fastest; the hypocenter location was estimated at 4 s after the origin time, and the threshold of the public warning in Japan was exceeded at 7 s. The warning area at 10 s is the largest among 3 methods. However, as the rupture propagates, the IPFx method underestimates the SI at the near-fault region in the southwest direction.

The PLUM method estimates the SI at each site from nearby stations. Therefore, the estimation error is the smallest compared to the methods using ground motion prediction equations (GMPE) for SI estimation. However, it is necessary to wait for the arrival of strong motions to nearby stations, so the warning time is shorter than other methods.

The XYtracker method captures the fault rupture dimension by the SI inversion. The method selects the point source model at the beginning and moves to the line source model at T = 60 s. The result of the XYtracker method is similar to that of the IPFx method at T<= 40 s, and approaches the result of the PLUM method after that with a slightly smaller estimate in the area close to the fault.

Figure 14 shows the observed vs estimated SIs by the IPFx, PLUM, and XYtracker method in the end. The IPFx method underestimates the observation, and the PLUM method overestimates especially in the area of high intensity. The XYtracker method has the smallest estimation error. However, for practical purposes, the false alarm by the overestimation is less critical than the missed alarm by the underestimation.

The results show that the point source approximation is reasonable until T = 40 s and the fault rupture cannot be negligible after that. The PLUM and XYtracker methods estimate the SI distribution better than the IPFx method after T=40s. The final SI distribution of the PLUM method is closer to the observed SI than the XYtracker method. This is mainly the consideration of the site effect. The PLUM method estimates the SI from the nearby stations, so the macroscopic site effect is included in the estimation. The IPFx and XYtracker methods assume no site effect since the site information in Turkey was not available. Consideration of the site amplification factor will improve the estimation accuracy of all three methods. Another factor affecting the estimation accuracy is the GMPE. We used the same GMPE used in the Japanese earthquake early warning

system to estimate a SI at a site. The ground motion attenuation has regionality and using a GMPE constructed from the Turkey dataset would improve the estimation accuracy.

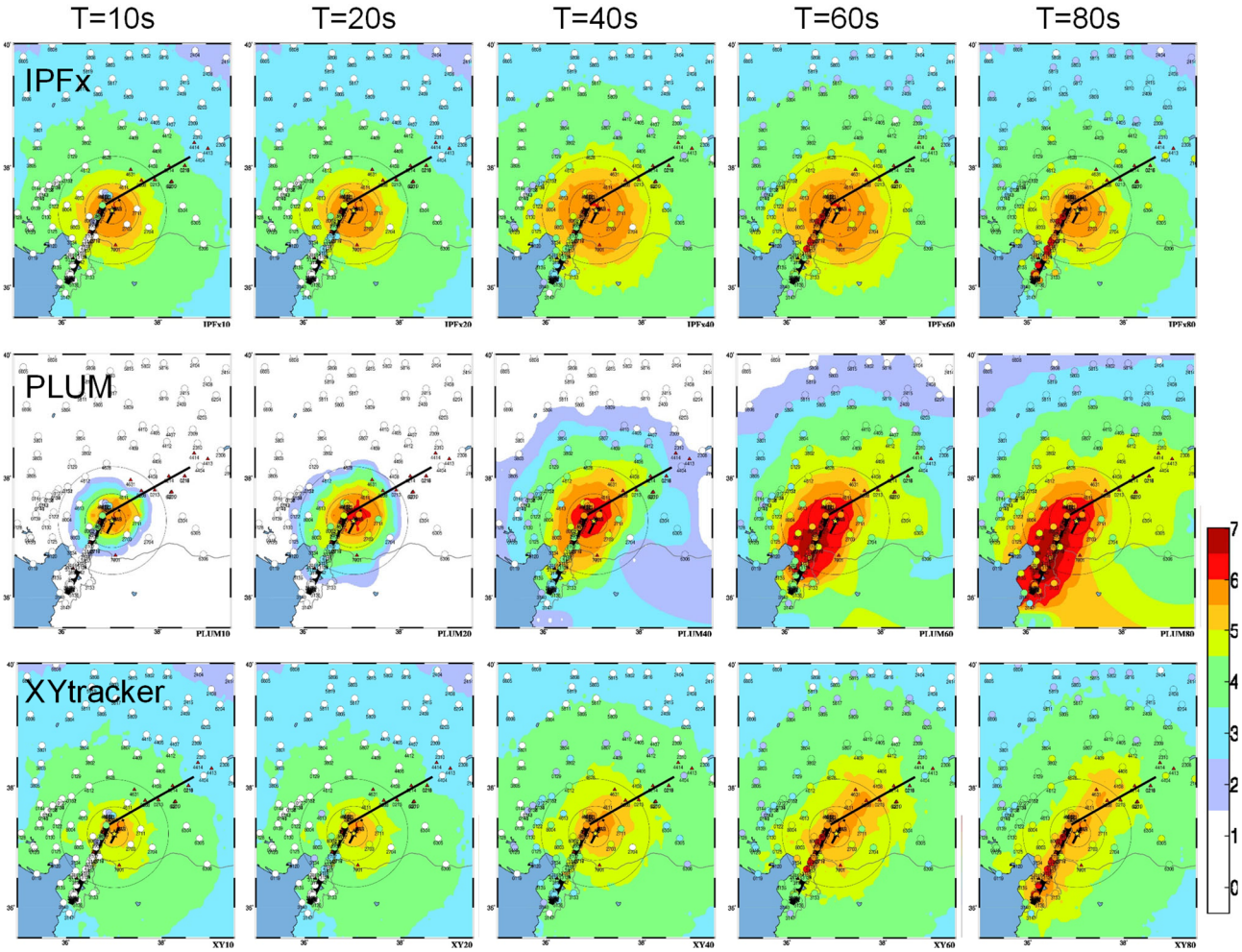

Figure 13 Snapshots of the estimated and observed SIs. The IPFx, PLUM, and XYtracker methods from the top. The time is at 10, 20, 40, 60, and 80 s from the left.

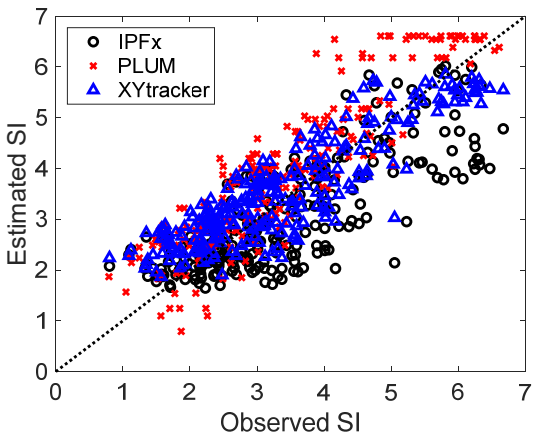

Figure 14 Observed vs estimated SIs from the IPFx, PLUM, and XYtracker methods.

6 Conclusions

We applied the three earthquake early warning methods to the 2023 Turkey-Syria earthquake (Mw 7.8) strong motion dataset.

The IPFx method estimates the hypocenter location and JMA magnitude. The hypocenter was estimated at 4 s after the origin time with the location error less than 10 km. Based on the JMA standard, the EEW may be able to be provided to the public at 7 s after the origin time. The blind zone (the area without warning before S-wave arrival) may be about 25 km.

The PLUM method estimates the wavefield from the observations of the nearby stations. We used the observations within 50 km from the target site and obtained about 10 s warning time. The ground motions are overestimated near the fault but the estimated SI captured the fault rupture extent.

The XYtracker method estimates the fault rupture dimension. It selects the most probable fault model out of three fault geometries by minimizing the AIC. For the Turkey-Syria earthquake, the PS model was selected up to 50 s and the LS model was dominant after that. The fault finiteness became critical 60 s after the origin time. The XYtracker method takes advantage of the previous two methods; the speed of the IPFx method and the accuracy of the PLUM method.

Assuming the strong motion data are available in real-time, these EEW methods can provide a warning to the public before the arrival of the severe shaking. However, this study is a theoretical simulation and assumes no data transmission latency. The speed of the data transmission and its robustness (no missing data) are critical for the EEW operation in the future.

7 References

Akaike, H. (1974) A new look at the statistical model identification. IEEE Trans Autom Control 19(6):716–723. https://doi.org/10.1109/TAC.1974.1100705

Böse M, Smith, D., Felizardo, C., Meier, M., Heaton, T., Clinton, J. (2018). FinDer vol 2: improved real-time ground-motion predictions for M2–M9 with seismic finite-source characterization. Geophys J Int 212(1):725–742. https://doi.org/10.1093/gji/ggx430

Hoshiba, M., Ohtake, K., Iwakiri, K., Aketagawa, T., Nakamura, H., and Yamamoto, S. (2010). How precisely can we anticipate seismic intensities? A study of uncertainty of anticipated seismic intensities for the earthquake early warning method in Japan, Earth Planets Space 62, 611-620, https://doi.org/10.5047/eps.2010.07.013

Japan Meteorological Agency (1996). Seismic Intensity, Gyosei, Tokyo, Japan, 238 pp. (in Japanese).

Japan Meteorological Agency (2020). Technical reference material on the overview and processing methods of earthquake early warning, https://www.data.jma.go.jp/svd/eew/data/nc/katsuyou/reference.pdf (in Japanese).

Kodera, Y., Yamada, Y., Hirano, K., Tamaribuchi, K., Adachi, S., Hayashimoto, N., Morimoto, M., Nakamura, M., Hoshiba, M. (2018). The Propagation of Local Undamped Motion (PLUM) Method: A Simple and Robust Seismic Wavefield Estimation Approach for Earthquake Early Warning. *Bulletin of the Seismological Society of America*, 108 (2): 983-1003. https://doi.org/10.1785/0120170085

Kunugi, T., Aoi, S., Nakamura, H., Suzuki, W., Morikawa, N., and Fujiwara, H. (2013). An improved approximating filter for real‐time calculation of seismic intensity, Zisin 2 65, 223-230, https://doi.org/10.4294/zisin.65.223 (in Japanese)

Liu, A. and M. Yamada (2014). Bayesian Approach for Identification of Multiple Events in an Early Warning System. Bulletin of the Seismological Society of America, 104(3), pp.1111-1121, https://doi.org/10.1785/0120130208

Liu, C., Lay, T., Wang, R. *et al.* (2023). Complex multi-fault rupture and triggering during the 2023 earthquake doublet in southeastern Türkiye. *Nat Commun* **14**, 5564, https://doi.org/10.1038/s41467-023-41404-5

Tamaribuchi, K., M. Yamada, and S. Wu (2014). A new approach to Identify Multiple Concurrent Events for Improvement of Earthquake Early Warning. Zisin: Journal of the Seismological Society of Japan, 67(2), pp.41-55, https://doi.org/10.4294/zisin.67.41 (in Japanese)

Xiao, Y. and M. Yamada (2022). XYtracker: a new approach to estimate fault rupture extent in real-time for large earthquakes. Earth Planets Space, 74, 77, https://doi.org/10.1186/s40623-022-01650-1

Yamada, M. and D.-Y. Chen (2022). Automatic Hypocenter Determination with the IPFx method for the 2018 Hualien earthquake sequence. Terrestrial, Atmospheric and Oceanic Sciences, 33:18. https://doi.org/10.1007/s44195-022-00018-y

Yamada, M. and J. Mori (2021). P-wave picking for earthquake early warning: Refinement of a Tpd method. Geophysical Journal International, 228(1), pp.387-395, https://doi.org/10.1093/gji/ggab349

Yamada, M., K. Tamaribuchi, and S. Wu (2021). IPFx: Extended integrated particle filter method for achieving high-performance earthquake early warning system. Bulletin of the Seismological Society of America, 111(3), pp.1263-1272, https://doi.org/10.1785/0120210008

8 Acknowledgements

We acknowledge the Disaster and Emergency Management Authority (AFAD) in Turkey for providing strong motion data (https://tdvms.afad.gov.tr/list-station/543428/37/37). This work was supported by the Ministry of Education, Culture, Sports, Science and Technology (MEXT) of Japan, under the STAR-E (Seismology TowArd Research innovation with data of Earthquake) Program Grant Number JPJ010217 and JSPS KAKENHI Grant Number JP 22K04652.